Applied Catalysis B: Environmental 237 (2018) 699–707

Contents lists available at ScienceDirect

Applied Catalysis B: Environmental

journal homepage: www.elsevier.com/locate/apcatb

Facile synthesis of graphene-phthalocyanine composites as oxygen reduction electrocatalysts in microbial fuel cells

Barbara Mecheri[a,*], Valerio C.A. Ficca[a], Maida Aysla Costa de Oliveira[a], Alessandra D'Epifanio[a], Ernesto Placidi[b,c], Fabrizio Arciprete[c], Silvia Licoccia[a]

[a] Department of Chemical Science and Technologies, University of Rome Tor Vergata, Via della Ricerca Scientifica, 00133, Italy
[b] CNR-ISM, Via Fosso del Cavaliere 100, I-00133, Rome, Italy
[c] Department of Physics, University of Rome "Tor Vergata", Via della Ricerca Scientifica, 00133, Italy

ARTICLE INFO

Keywords:
Graphene oxide
N-doping
Iron-phthalocyanine
Oxygen reduction reaction
Microbial fuel cells

ABSTRACT

In the path of direct energy conversion and wastewater disposal through microbial fuel cells (MFCs), the oxygen reduction reaction (ORR) plays a pivotal role. However, kinetic limitations hinders the spread of such technology requiring the use of a catalyst to develop efficient and cost effective devices. Herein we report a facile method for the preparation of iron-based catalyst supported on graphene oxide (GO) obtained by electrochemical exfoliation of graphite in aqueous solution of ammonium sulfate. Two different strategies to include nitrogen functionalities on/in GO matrix have been used, such as one-step nitrogen-doping in solution and post treatments based on annealing with ammonia gas. Iron (II) phthalocyanine (FePc) was used as iron source and deposited on GO by pyrolysis-free impregnation. Tuning the adjustable parameters governing the materials preparation allowed producing GO nanosheets with unique morphology and surface properties for enhancing the interaction with FePc. By combining the use of microscopy, electrochemical and spectroscopic techniques, a correlation between structure and surface chemistry of the prepared materials with catalytic activity towards ORR was established. The applicability of iron-based materials as ORR cathodes was evaluated by assembling single chamber air-cathodes MFCs, which power and voltage generation over time were acquired. The obtained results demonstrated that FePc/GO-based electrocatalysts can be used for electricity generation and waste treatment at the cathode side of MFCs.

1. Introduction

Anthropic impact on ecosystem is one of the most important topic of this century. With the aim of air and water pollution reduction, it is paramount to develop efficient energy conversion and waste disposal systems to support a greener way of life. On that purpose, microbial fuel cell (MFC) is an attractive technology suited for degrading organic pollutants while harvesting electrical energy at the same time [1–3]. In a typical MFC, the organics are oxidized into carbon dioxide, protons, and electrons by many different bacteria in anodic biofilms. Previous studies have demonstrated that exoelectrogenic bacteria, including Shewanella and Geobacter [4], are able to release electrons from the oxidation reaction outside the cell directly to the anode, where they move through the external circuit generating useful electricity. Due to high potential and natural abundance, oxygen is the most used oxidant at the cathode side. However, the operating conditions of MFCs, such as ambient temperature and neutral pH, severely limit the oxygen reduction reaction (ORR), resulting in high overpotential and slow kinetics. Hence, the use of catalysts is needed to accelerate ORR, but Platinum is not suitable for MFCs applications, being a rare and expensive metal, which can be deactivated in a polluted environment [5]. Many materials have been investigated as ORR catalysts in MFCs, such as bacterial catalysts [6], enzymes [7], and abiotic cathodes. Among abiotic cathodes, carbon nanostructures have been widely explored, due to high mechanical strength and electrical conductivities, high surface area, and tunable morphology and surface properties. Activated carbons, carbon nanotubes, nanofibers, and graphene have been frequently used as cathode catalysts in different types of MFCs. However, they allow achieving low power generation due to an intrinsic low ORR activities at neutral pH [8–11].

Platinum group metal-free (PGM-free) catalysts have proved to be a promising alternative to Pt due to their high activity in a neutral environment and good stability towards MFC fuels. Those catalysts, based on the coordination of a transition metal (M) with nitrogen in a carbon

* Corresponding author.
E-mail address: barbara.mecheri@uniroma2.it (B. Mecheri).

https://doi.org/10.1016/j.apcatb.2018.06.031
Received 27 February 2018; Received in revised form 7 June 2018; Accepted 11 June 2018
Available online 18 June 2018
0926-3373/

matrix, can be obtained by either pyrolysis of a metal salt (Co, Mn, Fe) and a nitrogen- and carbon-rich organic precursor [12–17] or integration of metal macromolecules having M–N bonds with carbon nanostructures [18–23]. Materials performance has been related to the content and type of nitrogen, to the coordination between metal and nitrogen, and surface properties and morphology of the conductive carbon support. Among carbon nanostructures, graphene oxide (GO) appears ideally suited as catalyst support: in fact, the presence of oxygen-containing surface groups and hydrophilicity increase availability of anchoring sites for catalyst particles and prevent the restack of graphene sheets [24,25]. Following the first report for the preparation of single-layer graphene [26], several approaches to fabricating graphene and GO have been developed: micromechanical cleavage [26], chemical vapor deposition [27], epitaxial growth [28] allow achieving high quality graphene, but the high cost and low production rate make such methods unsuitable for commercial applications. Chemical exfoliation allows reducing costs, but is still a time-consuming method, which involves the use of environmentally harmful chemicals and guarantees a lack of control on morphology [29]. By contrast, electrochemical exfoliation of graphite has been demonstrated to be an effective approach for preparing high quality graphene, at low cost and high production rate [30–32]. We report here a facile and efficient approach for large-scale preparation of ORR catalysts based on iron phthalocyanine (FePc) supported on nitrogen-doped GO. Insights on the effect of surface chemistry and morphology on catalytic activity have been achieved, and finally the catalyst has been applied at the cathode side of MFCs to evaluate application for power generation.

2. Experimental

2.1. Materials

2.1.1. Preparation of graphene oxide (GO)

GO was obtained by electrochemical exfoliation of graphite in a two-electrode cell. The working electrode was a graphite rod (GoodFellow, ϕ = 3 mm; L = 5 cm, particle size 20–100 μm, and purity 99%) and a counter electrode was a platinum wire (Amel Electrochemistry). The electrodes were immersed in an aqueous solution which composition is indicated in Table 1, applying a voltage in the 7–16 V range to promote graphite exfoliation. The obtained suspension was filtered under vacuum with a nylon membrane (pore size: 0.2 μm) and washed with DI. The powder was then dried in an oven at 70 °C for 12 h. When specified, the powder was also post-treated at 400 °C for 4 h under NH_3 flow.

2.1.2. Preparation of FePc/GO catalysts

0.5 g of GO were added to 30 mL of a methanol solution containing 17 mg mL^{-1} of FePc. The resulting mixture was stirred for 45 min. The mixture was heated in a water bath at 70 °C to evaporate methanol and the resulting powder was completely dried in an oven at 70 °C for 3 h, obtaining samples labeled as indicated in Table 1.

Table 1
Composition of the electrolyte solution used for graphite exfoliation, GO post treatment, and sample labeling.

Electrolytic solution	Post-treatment	Sample labeling	
		without catalyst	with catalyst
0.1 M $(NH_4)_2SO_4$	–	GO	FePc/GO
0.1 M $(NH_4)_2SO_4$ + 0.5 M NH_4OH	–	GO(N)_L1	FePc/GO(N)_L1
1 M $(NH_4)_2SO_4$ + 5 M NH_4OH	–	GO(N)_L2	FePc/GO(N)_L2
0.1 M $(NH_4)_2SO_4$	NH_3 gas	GO(N)_g	FePc/GO(N)_g

2.2. Methods

2.2.1. Materials characterization

Atomic Force Microscopy (AFM) was carried out in air using a Veeco Multiprobe IIIa instrument. Experiments were carried out in tapping mode by using Si tips with a spring constant of about 40 N/m and a typical curvature radius on the tip of 7 nm. All samples were dispersed in DI to a 0.01 mg mL^{-1} content and deposited on freshly cleaved Mica substrates.

Raman Spectroscopy was performed with a DXR Raman Microscope (Thermo Scientific) using laser excitation wavelength of 532 nm with a 10 X objective. Laser power was maintained at 0.1 mW. Experimental data were fitted using OMNIC™ Series Software.

Fourier Transform Infrared Spectroscopy (FTIR) was carried out by means of a FTIR100 spectrometer (Perkin Elmer) in transmittance mode. Samples were pelleted in 150 mg of KBr using a Specac manual hydraulic press, by applying a pressure of 7 tons for 5 min. The diameter of pellets was 13 mm.

X-ray Photoelectron Spectroscopy (XPS) was performed using an Omicron DAR 400 A l/Mg Kα nonmonochromatized X-ray source, and a VG-CLAM2 electron spectrometer. Samples were dispersed in ethanol to a 1 mg mL^{-1} content and deposited on silicon wafer.

Cyclic Voltammetry (CV) was carried out by using a VMP3 Potentiostat (Bio Logic Science Instruments) controlled by computer through EC-Lab V10.18 software. A conventional three electrode cell was used: the reference electrode was a saturated calomel electrode-SCE, (Amel 303/SCG/12), the auxiliary electrode was a platinum wire (Amel, 805/SPG/12), and the working electrode (WE) was a glassy carbon disk (GC, 0.196 cm^2 area) modified with catalyst layer. The catalyst layer was prepared by dispersing either GO or FePc/GO (4 mg) in 270 μL of ethanol and 135 μL of DI. This dispersion was treated in an ultrasonic bath for 30 min. Then, 50 μL of Nafion solution (5 wt. % in lower aliphatic alcohols and water, Aldrich) were added to the dispersion and vortexed for 2 min. An aliquot of the resulting dispersion was deposited on the GC electrode to a catalyst loading of 0.27 $mgcm^{-2}$ (corresponding to 0.013 $mgcm^{-2}$ iron loading in the case Fe-based composites) and dried at 40 °C for 4 min.

CV experiments were carried out at room temperature in 100 mM neutral phosphate buffer solution (PBS), saturated with either nitrogen or oxygen. Each tests consisted in 5 cycles, CV curves shown in the manuscript refer to the 5th cycle (scan rate 5 mVs^{-1}). Linear Sweep Voltammetry was carried out in O_2-saturaeted PBS at a scan rate of 5mVs^{-1}. Electrical double-layer capacitance (CDL) of GO sheets was estimated by recording CV curves in N_2-saturated atmosphere and measuring the capacitive current at 0.95 V in the absence of faradic contribution at different scan rates (5, 10, 25, 50, and 100 mVs^{-1}). CDL was obtained from slope of linear plot of capacitive current vs scan rate [10,33]. All potential values in the manuscript were measured vs. SCE and then converted to the reversible hydrogen electrode (RHE) scale.

2.2.2. Tests in microbial fuel cells

MFC cathodes were prepared by modifying carbon cloth electrodes with the diffusion layer (exposed to air) and the catalyst layer (faced to MFC solution). The diffusion layer was prepared as previously described [34,35]. The deposition of the catalyst layer was carried out on the opposite side of the diffusion layer by brushing a suspension prepared from 64 $mgmL^{-1}$ of either GO or FePc/GO in a mixture containing DI, Nafion solution, and 2-propanol (1:8:4, as volume ratio). The electrodes were dried at room temperature for 24 h. The catalyst loading was 10 $mgcm^{-2}$ (corresponding to 0.5 $mgcm^{-2}$ iron loading in the case of FePc/GO cathodes).

MFC cathodes (diameter 4 cm) were assembled in a single-chamber air-cathode MFC (inner volume: 28 mL) which anode was a graphite fiber brush. MFCs were firstly acclimated as described before [36] and fed with phosphate buffer solution containing 1 g L^{-1} of sodium acetate. Polarization and power density curves were acquired by

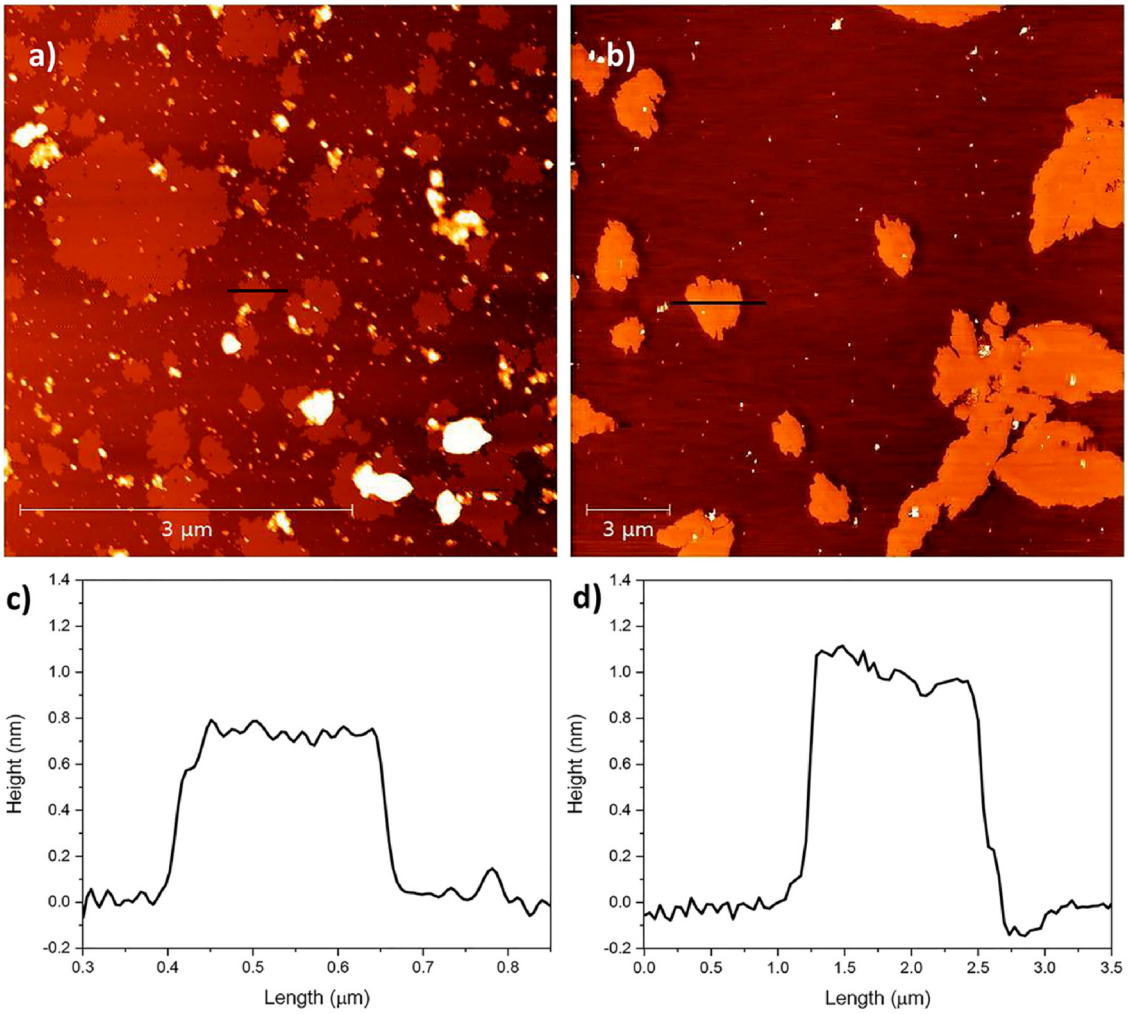

Fig. 1. AFM images of (a) GO(N)_L1, (b) GO(N)_L2, and height profiles of (c) GO(N)_L1, and (d) GO(N)_L2 samples.

varying the external resistance (10–10000 Ohm) every 30 min and measuring the cell voltage at each resistance. All the measurements were carried out at room temperature (20 ± 3 °C), acquiring two independent replicates for each cathode.

3. Results and Discussion

3.1. Characterization of GO

AFM was used to carry out an in-depth investigation on morphology, surface area, and thickness of GO layers. Fig. 1 shows the AFM images and the height profiles of two representative samples of the series (GO(N)_L1 and GO(N)_L2).

GO(N)_L1 consists of small sheets (0.2–1 μm^2 surface area) with a regular shape and smooth edges. Few large sheets (surface area < 10 μm^2) with irregular shape can be also seen. As shown in Fig. 1c, GO(N)_L1 has a smooth thickness with an average value of 0.79 nm. The morphology of GO(N)_L2 is similar to that of GO(N)_L1, while irregularly shaped sheets can be found in both GO and GO(N)_g samples.

The major difference between GO and GO(N)_g is that GO(N)_g sheets have smoother edges and a more homogeneous basal plane with respect to GO. Such a difference can be ascribed to the thermal treatment of the GO(N)_g, allowing the basal plane of the sheets to be partially restored. Concerning thickness of the sheets, for all samples can be found sheets with thickness in the 0.8–1.0 nm range. Considering that the interlayer distance of graphite oxide ranges between 0.6–1.2 nm depending on the hydration degree, the thickness of all GO sheets is 1–2 monolayers [37].

Fig. 2a shows the Raman spectra of GO samples. Previous research showed that the typical fingerprint of crystalline graphene consists in the G (~ 1585 cm^{-1}) and the 2D bands (~ 2700 cm^{-1}), originated from the first- and second- order allowed Raman mode E2g, respectively [38,39].

Fig. 2a shows the appearance of the disorder-induced D band at ~1350 cm^{-1} and some changes in the position of G and 2D bands with respect to crystalline graphene. In particular, the 2D band is split into an increasing number of modes (D + G at 2930 cm^{-1}, and G + D' at 3150 cm^{-1}), and the G band was blue shifted as indicated in Table 2. Moreover, the presence of a shoulder between G and D band can be seen in all samples. These features are consistent with fewer-layered graphene oxide, also characterized by the presence of structural defects [40,41].

The deconvolution of Raman spectra allows evaluating the degree of structural disorder in the GO samples. According to previous reports [42], the Raman spectra in the shaded area of Fig. 2a fit to five functions which can be ascribed to G, D, D', D*, and D" bands, and Fig. 2b shows an example of deconvolution obtained for the GO(N)_L1 sample. In particular, the D band is related to the A1g breathing mode due to the modification of the basal plane structure of graphene induced by defects [43]. Moreover, the D" band can be also ascribed to the presence of interstitial defects and lack of crystallinity induced by graphite [44,45]. Then, ID/IG and ID"/IG intensity ratio can be used to evaluate the degree of the disorder in the sample, which is also related to the density functional groups anchored on the framework [42,46]. The

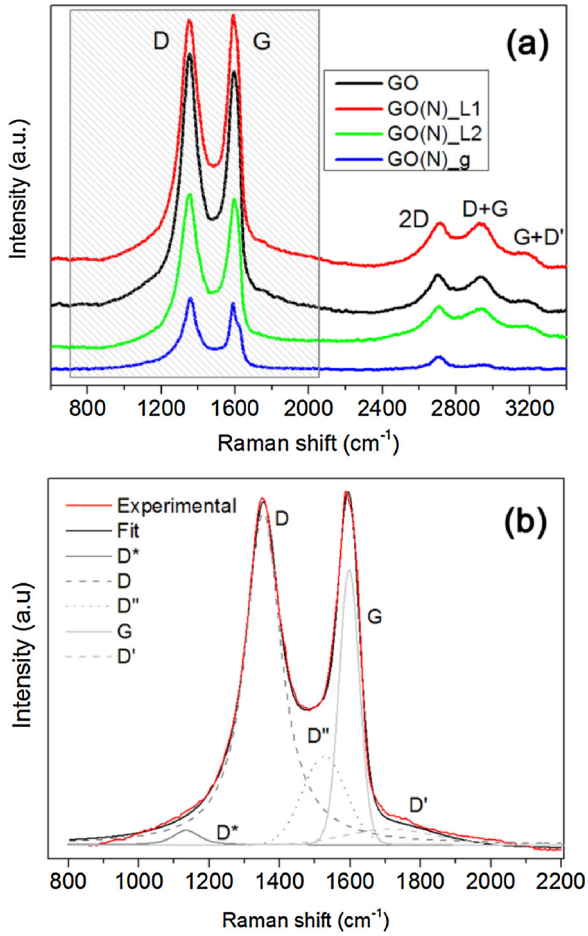

Fig. 2. (a) Raman spectra of GO, GO(N)_L1, GO(N)_L2, and GO(N)_g; (b) A typical five function (D*,D, D", G, and D' bands) fit for GO(N)_L1 sample.

Table 2
Position of D, D", and G bands of GO samples; I(D)/I(G) and ID"/IG are the ratio between the heights of the corresponding peaks.

Sample	D band (cm^{-1})	D" band (cm^{-1})	G band (cm^{-1})	ID/IG	ID"/IG
GO	1353	1520	1598	1.15	0.23
GO(N)_L1	1353	1527	1597	1.21	0.32
GO(N)_L2	1352	1527	1600	1.16	0.27
GO(N)_g	1357	1504	1588	1.18	0.19

values of I(D)/I(G) and ID"/IG ratio point out that the defect concentration and oxygen content is the lowest for GO(N)_g and the highest for GO(N)_L1 and GO(N)_L2.

Surface chemistry of GO samples was investigated by XPS. Table 3 shows the elemental analysis of the samples, which mainly consist of carbon. The oxygen content is significantly high for GO and GO(N)_L1, while for GO(N)_L2 and GO(N)_g oxygen content is reduced.

Analysis and deconvolution of the C1s peak (Fig. 3a) results in seven component peaks corresponding to C—C and C—H (284.5 eV), C—O and C═N (285.8 eV), C═O and C–N (287.1 eV), O—C = O (288.6 eV), and π–π* shake up satellite [47]. For all samples (with the exception of GO (N)_g), oxygen-containing surface groups are mainly distributed in the hydroxyl group, demonstrated in Table 3.

Hence, GO(N)_g has the lowest oxygen content and relative density of −OH groups, in agreement with FTIR results (Fig. S1). For nitrogen, N1s spectrum fits to four functions (Fig. 3b), corresponding to pyridinic (398.3 eV), amine moieties (399.3 eV), pyrrolic (400.5 eV), and quaternary/graphitic nitrogen (401.7 eV) [48]. All types of nitrogen were found in all samples, amine moieties being predominant in all cases. The main difference among the samples is the graphitic to pyridinic nitrogen ratio which is much higher for GO and GO(N)_L1 as compared to GO(N)_L2 and GO(N)_g.

The capacitive behavior of GO sheets was evaluated by cyclic voltammetry under nitrogen purging at different scan rates, obtaining electrode double-layer capacitance, C_{DL} (Figure S2). Both structure and morphology of the electrode surface affect C_{DL}, which is expected to increase with increasing of electrochemical accessible area [10,22,33,49]. For all samples C_{DL} values are listed in Table 4. GO(N)_g has the lowest C_{DL}, suggesting that this sample has the lowest surface area.

The catalytic activity of GO sheets towards ORR was also evaluated by CV (Fig. 4). While no faradic peaks were detected under N_2 purging, all samples showed a well-defined reduction peak when the electrolyte solution is saturated with oxygen.

This finding indicates that all samples show catalytic activity towards ORR. Among the series of samples, the reduction peak is centered at around 0.4 V for GO, GO(N)_L1, and 0.45 V for GO(N)_L2 samples, while the peak is shifted towards less positive potential (0.25 V) for GO (N)_g. In addition, GO(N)_g displays the lowest peak current density (Table 4). Linear sweep voltammetry (LSV) with rotating disk electrode was also carried out, and Figure S3 shows LSV curves at different electrode rotation rate for a representative sample of the series.

Both CV and LSV measurements converge to indicate that GO(N)_g is the less effective sample towards ORR catalysis. This can be ascribed to the interplay of morphology and surface chemistry on the electrochemical properties. The reduced surface area of GO(N)_g sample is indeed a factor contributing to low catalytic activity towards ORR. As far as surface chemistry is concerned, XPS results highlighted that the density of both nitrogen and hydroxyl groups is the lowest for GO(N)_g sample. In neutral media, nitrogen and oxygen functionalities, in particular hydroxyl groups, were found to play a key role on ORR catalysis [50,51], for they act as active sites for O_2 adsorption and electron transfer. As previously reported [52], the stronger the bond between the catalyst and the adsorbed molecule, the more efficient is the charge transfer. In the case of our samples, we suggest that a high density of surface hydroxyl groups enables cutting the pathway of the ORR moving or reducing the rate determining step (RDS). According to Table S1, the RDS for ORR on carbon materials is represented by the first electron transfer and the first protonation to the adsorbed O_2 molecule both required to break the double bond of O_2. The presence of hydroxyl groups allows a faster ORR process with a forward starting point compared to the normal pathway. Also, nitrogen functionalities in the GO framework have a synergistic effect with oxygen functionalities on ORR, the first ones acting as active sites for O_2 adsorption while the latter in further decreasing the activation energy of ORR. This mutual

Table 3
Elemental analysis obtained by XPS and chemical speciation of oxygen and nitrogen atoms on GO structure.

Sample	C (At.%)	O (At.%)	-OH (Rel.%)	N (At.%)	Npyrid (Rel.%)	Namin (Rel.%)	Npyrro (Rel.%)	Ngra (Rel.%)	Ngra/Npyrid
GO	83.6	15.5	52.8	0.9	14.9	41.3	30.6	13.2	0.91
GO(N)_L1	83.4	14.1	46.6	2.5	20.1	37.6	23.7	18.6	0.93
GO(N)_L2	89.8	7.4	42.0	2.8	24.5	44.3	25.3	5.9	0.24
GO(N)_g	95.6	2.6	–	1.8	27.6	30.9	27.3	14.2	0.51

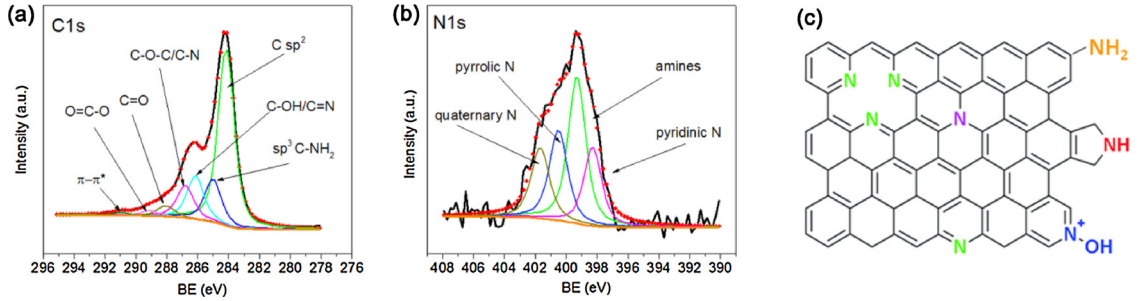

Fig. 3. C1s (a), N1s (b) spectra of GO(N_L1) as a representative sample of the series. Typical speciation of nitrogen atom in GO sheets (c).

Table 4
Electrochemical parameters extrapolated by CV analysis; CDL (electrode double-layer capacitance), Jp (current density of ORR peak), Ep (ORR peak potential).

Sample	*without FePc*			*with FePc*		
	C_{DL} ($mFcm^{-2}$)	Jp ($mAcm^{-2}$)	Ep (V)	C_{DL} ($mFcm^{-2}$)	Jp ($mAcm^{-2}$)	Ep (V)
GO	13.6	0.31	0.42	2.62	0.23	0.72
GO(N)_L1	9.9	0.26	0.38	5.84	0.24	0.73
GO(N)_L2	18.1	0.36	0.46	3.46	0.21	0.65
GO(N)_g	2.82	0.20	0.24	1.12	0.06	0.68

effect explains the difference in the activity of the GO samples explaining the reason why the lowest OH and nitrogen contents of GO(N)_g are responsible of the poorest electrocatalytic activity towards ORR of this material.

3.2. Preparation and characterization of FePc/GO catalysts

To boost catalytic activity towards ORR, iron phthalocyanine (FePc) was supported on GO nanosheets as described in the experimental section. AFM images demonstrated that FePc/GO composites have a morphology similar to that of pristine GO sheets (Fig. S4), maintaining the intrinsic thickness of about 1 nm. We also acquired CVs of FePc/GO samples in both N_2 and O_2 saturated electrolyte (Fig. S5). As shown in Table 4, the deposition of FePc on GO supports results in a decrease in CDL and Jp values; by contrast, the position of the oxygen reduction potential experiences a significant positive shift for all samples, indicating catalytic activity towards ORR of GO nanosheets is enhanced by FePc. In particular, FePc/GO and FePc/GO(N)_L1 have the highest catalytic activity towards ORR, as indicated by the highest Jp and more positive Ep values.

The superior catalytic activity of FePc/GO and FePc/GO(N)_L1 complexes can be explained in terms of an enhanced FePc-GO interaction compared to FePc/GO(N)_L2 and FePc/GO(N)_g. Oxygen- and nitrogen surface groups play indeed a key role on iron coordination and thus on catalytic activity towards ORR. In particular, oxygen functionalities on GO surface (especially, hydroxyl and carbonyl groups) enable coordinative binding of iron cations, acting as an axial ligand [53]. Such donor (FePc) – acceptor (GO) interaction results in an enhanced electron density of oxygen-groups on GO surface after the introduction of FePc moieties. Moreover, the graphitic domains of GO,

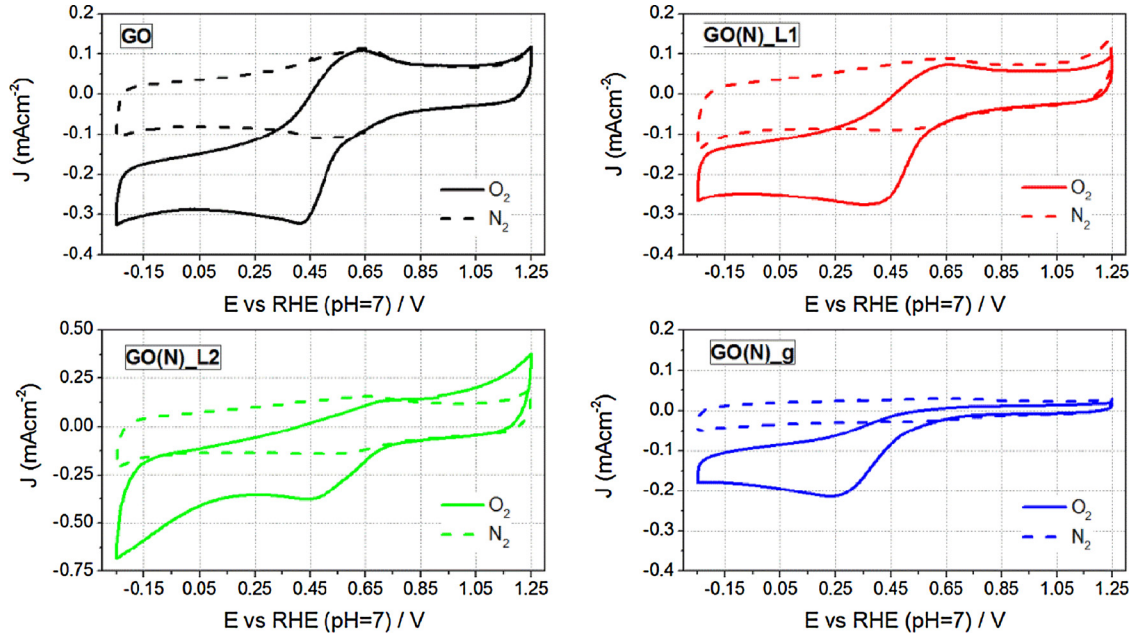

Fig. 4. CV curves of GO, GO(N)_L1, GO(N)_L2, and GO(N)_g in N_2-(dotted line) and O_2-saturated (solid line) 100 mM neutral phosphate buffer solution. Scan rate: $5mVs^{-1}$.

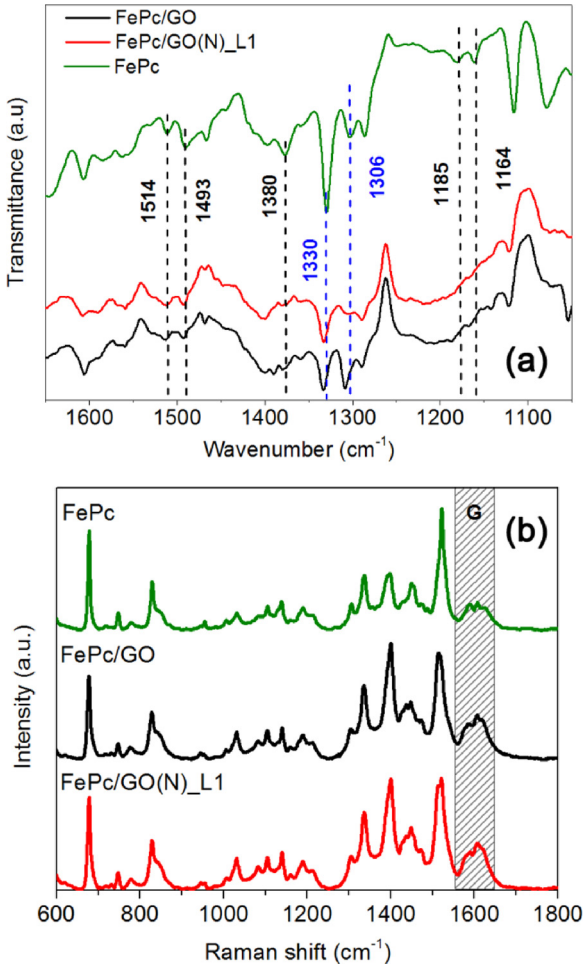

Fig. 5. FTIR (a) and Raman (b) spectra of FePc, FePc/GO, and FePc/GO(N)_L1.

Table 5
Elemental composition and element speciation for FePC/GO and FePc/GO(N)_L1 composites.

Sample	Carbon (At.%)	Oxygen (At.%)	OH (Rel. %)	Nitrogen (At.%)	Ngra (Rel.%)	Iron (At. %)	Fe(II) (Rel. %)	Fe (III) (Rel. %)
FePc/GO	80.5	8.2	68.2	10.8	2.0	0.5	67.1	32.9
FePc/GO(N)_L1	79.8	8.6	67.0	11.1	1.8	0.5	60.1	39.9

mainly composed by sp^2 carbon, is also able to interact with the phthalocyanine ring through pi-stacking interactions with the graphitic nitrogen contributing to enhance the interaction [54,55]. As highlighted by XPS analysis, GO and GO(N)_L1 have the highest graphitic to pyridinic nitrogen ratio and high density of hydroxyl surface groups, enabling a strong interaction between FePc and GO. This finding explains the superior ORR activity of FePc/GO and FePc/GO(N)_L1 compared to FePc/GO(N)_L2 and FePc/GO(N)_g.

To get deeper insights on the nature of FePc/GO interactions, FTIR spectra of the complexes were acquired and compared to that of unsupported FePc (Fig. 5a).

Unsupported FePc shows the typical FTIR spectrum of metal phthalocyanine [56–59]. Supporting of FePc on graphene oxide resulted in decreased intensity, shift and eventual disappearance of some FTIR bands in the spectra of FePc/GO and FePc/GO(N)_L1. The dashed lines in Fig. 5a indicate the modified and missing bands, which can be assigned to the vibrations of FePc bonds involving both the central Fe ions and the N4-macrocycle (Table S2). The modifications of FTIR transmittance bands after FePc deposition on GO is a consequence of the interaction between FePc and the basal plane of graphene oxide which hiders FePc bonds vibrations. In particular, the modification of the bands at 1330 and 1306 cm^{-1} is more evident for FePc/GO(N)_L1 than FePc/GO, as a results of a stronger interaction which could be favored by the higher density of nitrogen.

In Fig. 5b, Raman spectra of composites confirm the support/catalyst interaction through a shift of the peak at 1600 cm^{-1} corresponding to the Raman active modes originating from G band of GO. Due to π-π interaction between FePc and graphene, the G-band was red shifted by 8 cm^{-1} and 11 cm^{-1} for FePc/GO and FePc/GO(N)_L1, respectively. In particular, the higher shift for the GO (N)_L1 sample indicates the active role of nitrogen in maximizing the support/catalyst interaction [54,60].

The XPS data of elemental composition of FePc/GO and FePc/GO(N)_L1 composites are given in Table 5. Both composites consist mainly of carbon, with the presence of comparable quantities of oxygen, nitrogen, and iron.

Fig. 6 shows the analysis and deconvolution of the C1s, N1s, and Fe2p peaks for FePc/GO(N)_L1 as a representative sample of the series. Carbon, nitrogen and iron speciation was derived by the fitting, which corresponding parameters are listed in Table 5, for the most representative functionalities. The full deconvolution parameters are listed in Table S3.

As a first remark, the chemical composition of FePc/GO(N)_L1 is similar to that of pristine GO(N)_L1 in terms of oxygenated and nitrogenated groups. The N1s peaks was fitted to four components, and the band at 401.1 eV, corresponding to graphitic N, experienced a shift to higher binding energy compared to that in pristine GO(N)_L1 (Δ(BE) = 0.6 ± 0.1 eV). The same behaviour was seen for FePc/GO. By contrast, the N1s XPS spectrum of unsupported FePc does not show any evidence of graphitic nitrogen (Figure S6). The presence of graphitic nitrogen and the binding energy shift of the corresponding XPS peak further demonstrate the expression of π-π interactions due to

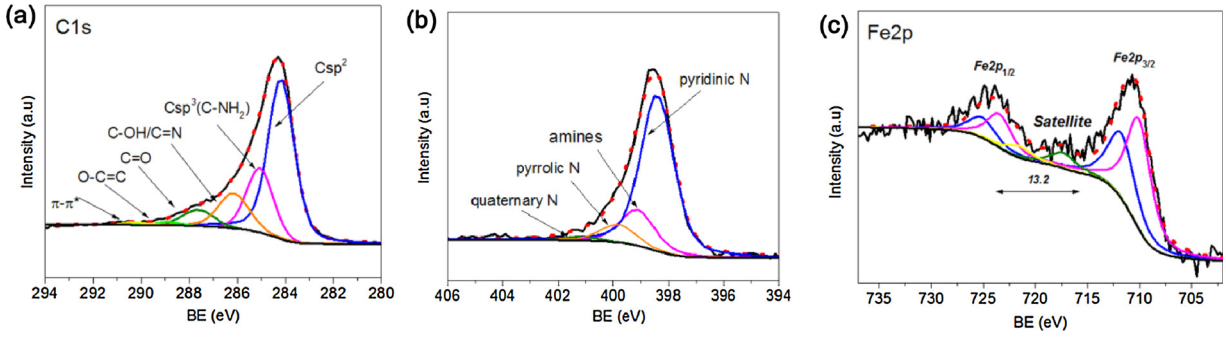

Fig. 6. C1s (a), N1s (b), and (c) Fe2p XPS spectra of FePc/GO(N)_L1.

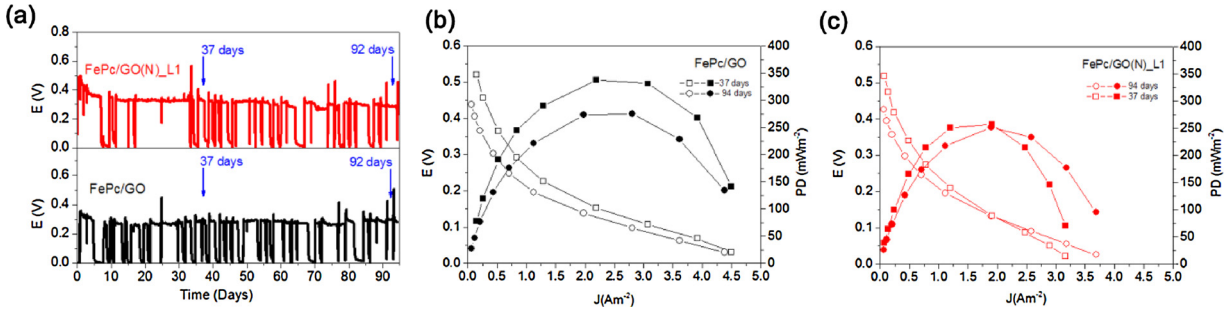

Fig. 7. Voltage generation cycles under R_{ext} = 1000 Ohm (a), and Polarization and power density (right) curves of MFC assembled with FePc/GO(N)_L1 (b) and FePc/GO (c) as cathodes taken after 37, and 94 days from acclimation. Feeding: $NaC_2O_2H_3$ (1 g L^{-1}) in neutral phosphate buffer.

Table 6
Performance of MFCs assembled with Fe- and Pt-based cathodes.

Cathode	Average E @1 kΩ (V)	PD_{max} (mWm^{-2})	J@0.2 V (Am^{-2})
FePc/GO	0.28	280	1.2
FePc/GO(N)_L1	0.30	260	1.2
Pt/C	0.38	230	1.0

charge transfer from FePc to graphene in the composite [61,62].

As far as iron is concerned, Fe is present as ferric and ferrous ion in both composites and unsupported FePc, the ferrous state being dominant for all samples. Beside parasitic oxidation, the presence of ferric ion can be ascribed to the donor-(FePc) acceptor-(GO) interaction promoted by both OH groups and graphitic nitrogen on GO supports. The highest Fe(III) relative content of GO(N)_L1 is an indication of a stronger FePc/support interaction as compared to FePc/GO.

3.3. MFC tests

To evaluate the electrochemical performance in terms of MFC voltage and power generation, FePc/GO(N)_L1 and FePc/GO were assembled at the cathode side of MFC prototypes. Fig. 7a shows voltage generation cycles, indicating that both cells allow achieving high and stable voltage over 90 days. The average voltage is 0.32 V and 0.28 V for FePc/GO(N)_L1 and FePc/GO cathode, respectively.

Figs. 7b and c show polarization and power density curves taken after 37 and 92 days after acclimation for FePc/GO(N)_L1 and FePc/GO as cathodes. The maximum power density and the corresponding current density are higher than 250 mW m^{-2} and 1.9 Am^{-2} for both cells in the whole period considered.

Table 6 summarized the electrochemical performance, together with that of a MFC equipped with a reference Pt/C cathode [22].

The performance of iron-based catalysts is consistent and even outperforms previously reported performance of MFCs assembled with cathodes based on graphene, activated carbons or carbon supported metal macrocycles [21,22,63,64]. Also, iron-based cathodes allow generating electrical power as high as that of Pt-based cathodes.

The comparison between the performance of the two FePc-based cathodes underlines that the FePc/GO cathode undergoes up to a maximum PD loss of 20%, while for FePc/GO(N)_L1 the loss is lower than 1%, indicating a superior stability of FePc/GO(N)_L1 with respect to FePc/GO under MFC operation. This finding can be ascribed to the enhanced interaction between FePc and GO(N)_L1 support which promoted by both OH groups and graphitic nitrogen on GO(N)_L1 support, as highlighted in the discussion of Raman and XPS results.

4. Conclusions

Electrochemical exfoliation of graphite in aqueous solution of ammonia and ammonium sulphate is a facile, efficient and up scalable technique to produce N-functionalized graphene oxide (GO).

Tuning the exfoliation parameters and solution composition allowed the production of GO nanosheets with peculiar features, such as smooth edges, regular shape, and homogeneous thickness. Thanks to the high surface density of −OH groups and graphitic nitrogen, introduced without any post treatment at high temperature, is possible to obtain a suitable catalytic support to iron phthalocyanine (FePc). Indeed a good combination of morphology and surface chemistry is fundamental to enhance the interaction of GO and FePc and to boost catalytic activity towards ORR. Among a rich diversity of oxygen containing surface groups, hydroxyl groups possess a dual role of cutting the ORR pathway on GO surface and enhance the FePc bonding with the GO support. The interaction between FePc and the GO support is further promoted by the presence of graphitic N, as demonstrated by FTIR, Raman and XPS.

Among the set of samples prepared, the FePc/GO and FePc/GO(N)_L1 composites return the best results in terms of enhanced catalytic activity and catalyst stabilization, as demonstrated by CV and MFC tests. For those samples, cyclic voltammetries at neutral pH gave the highest current density and more positive peak potential for oxygen reduction. Compared to previously reported materials, the key feature of FePc/GO systems is that they can be synthesized by using mild conditions, without relying on time consuming and expensive high-temperature approaches for their preparation.

When assembled at the cathode side of MFCs, the performance of FePc/GO and FePc/GO(N)_L1 composites, in terms of maximum power and current density, outperforms previously reported performance of MFCs assembled with either Pt-based cathodes or platinum group metal-free cathodes.

Acknowlegments

The present work was carried out with the support of the “European Union's Horizon 2020 research and innovation programme”, under H2020-FTIPilot-2015-1 (Grant Agreement n. 720367-GREENERNET) and CNPq - Conselho Nacional de Desenvolvimento Científico e Tecnologico, Brazil, under the grant n.200631 - 2015/2. Thanks are due to Ms. Cadia D'Ottavi for her valuable technical support.

Appendix A. Supplementary data

Supplementary material related to this article can be found, in the online version, at doi:https://doi.org/10.1016/j.apcatb.2018.06.031.

References

[1] A. Rinaldi, B. Mecheri, V. Garavaglia, S. Licoccia, P. Di Nardo, E. Traversa, Engineering materials and biology to boost performance of microbial fuel cells: a critical review, Energy Environ. Sci. 1 (2008) 417, http://dx.doi.org/10.1039/b806498a.
[2] C. Santoro, C. Arbizzani, B. Erable, I. Ieropoulos, Microbial fuel cells: from fundamentals to applications. A review, J. Power Sources 356 (2017) 225–244, http://dx.doi.org/10.1016/J.JPOWSOUR.2017.03.109.
[3] T. Pepe Sciarria, G. Merlino, B. Scaglia, A. D'Epifanio, B. Mecheri, S. Borin, S. Licoccia, F. Adani, Electricity generation using white and red wine lees in air

cathode microbial fuel cells, J. Power Sources 274 (2015) 393–399, http://dx.doi.org/10.1016/j.jpowsour.2014.10.050.
[4] B.E. Logan, Exoelectrogenic bacteria that power microbial fuel cells, Nat. Rev. Microbiol. 7 (2009) 375–381, http://dx.doi.org/10.1038/nrmicro2113.
[5] F. Harnisch, S. Wirth, U. Schröder, Effects of substrate and metabolite crossover on the cathodic oxygen reduction reaction in microbial fuel cells: platinum vs. Iron(II) phthalocyanine based electrodes, Electrochem. Commun. 11 (2009) 2253–2256, http://dx.doi.org/10.1016/J.ELECOM.2009.10.002.
[6] L. Rago, P. Cristiani, F. Villa, S. Zecchin, A. Colombo, L. Cavalca, A. Schievano, Influences of dissolved oxygen concentration on biocathodic microbial communities in microbial fuel cells, Bioelectrochemistry 116 (2017) 39–51, http://dx.doi.org/10.1016/j.bioelechem.2017.04.001.
[7] C. Santoro, S. Babanova, P. Atanassov, B. Li, I. Ieropoulos, P. Cristiani, High power generation by a membraneless single chamber microbial fuel cell (SCMFC) using enzymatic bilirubin oxidase (BOx) air-breathing cathode, J. Electrochem. Soc. 160 (2013) H720–H726, http://dx.doi.org/10.1149/2.058310jes.
[8] X. Zhang, X. Xia, I. Ivanov, X. Huang, B.E. Logan, Enhanced activated carbon cathode performance for microbial fuel cell by blending carbon black, Environ. Sci. Technol. 48 (2014) 2075–2081, http://dx.doi.org/10.1021/es405029y.
[9] G. Pasternak, J. Greenman, I. Ieropoulos, Comprehensive study on ceramic membranes for low-cost microbial fuel cells, ChemSusChem 9 (2016) 88–96, http://dx.doi.org/10.1002/cssc.201501320.
[10] C. Santoro, M. Kodali, S. Kabir, F. Soavi, A. Serov, P. Atanassov, Three-dimensional graphene nanosheets as cathode catalysts in standard and supercapacitive microbial fuel cell, J. Power Sources 356 (2017) 371–380, http://dx.doi.org/10.1016/j.jpowsour.2017.03.135.
[11] X. Yang, W. Zou, Y. Su, Y. Zhu, H. Jiang, J. Shen, C. Li, Activated nitrogen-doped carbon nanofibers with hierarchical pore as efficient oxygen reduction reaction catalyst for microbial fuel cells, J. Power Sources 266 (2014) 36–42, http://dx.doi.org/10.1016/j.jpowsour.2014.04.126.
[12] W. Yang, B.E. Logan, Immobilization of a metal-nitrogen-carbon catalyst on activated carbon with enhanced cathode performance in microbial fuel cells, ChemSusChem 9 (2016) 2226–2232, http://dx.doi.org/10.1002/cssc.201600573.
[13] L. Birry, P. Mehta, F. Jaouen, J.-P. Dodelet, S.R. Guiot, B. Tartakovsky, Application of iron-based cathode catalysts in a microbial fuel cell, Electrochim. Acta. 56 (2011) 1505–1511, http://dx.doi.org/10.1016/J.ELECTACTA.2010.08.019.
[14] F. Zhao, F. Harnisch, U. Schröder, F. Scholz, P. Bogdanoff, I. Herrmann, Application of pyrolysed iron(II) phthalocyanine and CoTMPP based oxygen reduction catalysts as cathode materials in microbial fuel cells, Electrochem. Commun. 7 (2005) 1405–1410, http://dx.doi.org/10.1016/J.ELECOM.2005.09.032.
[15] C. Santoro, A. Serov, R. Gokhale, S. Rojas-Carbonell, L. Stariha, J. Gordon, K. Artyushkova, P. Atanassov, A family of Fe-N-C oxygen reduction electrocatalysts for microbial fuel cell (MFC) application: relationships between surface chemistry and performances, Appl. Catal. B Environ. 205 (2017) 24–33, http://dx.doi.org/10.1016/J.APCATB.2016.12.013.
[16] S. Rojas-Carbonell, C. Santoro, A. Serov, P. Atanassov, Transition metal-nitrogen-carbon catalysts for oxygen reduction reaction in neutral electrolyte, Electrochem. Commun. 75 (2017) 38–42, http://dx.doi.org/10.1016/J.ELECOM.2016.12.011.
[17] M. Kodali, C. Santoro, A. Serov, S. Kabir, K. Artyushkova, I. Matanovic, P. Atanassov, Air breathing cathodes for microbial fuel cell using Mn-, Fe-, Co- and Ni-containing platinum group metal-free catalysts, Electrochim. Acta 231 (2017) 115–124, http://dx.doi.org/10.1016/J.ELECTACTA.2017.02.033.
[18] F. Harnisch, N.A. Savastenko, F. Zhao, H. Steffen, V. Brüser, U. Schröder, Comparative study on the performance of pyrolyzed and plasma-treated iron(II) phthalocyanine-based catalysts for oxygen reduction in pH neutral electrolyte solutions, J. Power Sources 193 (2009) 86–92, http://dx.doi.org/10.1016/j.jpowsour.2008.12.049.
[19] A. Iannaci, B. Mecheri, A. D'Epifanio, M.J. Lázaro Elorri, S. Licoccia, Iron–nitrogen-functionalized carbon as efficient oxygen reduction reaction electrocatalyst in microbial fuel cells, Int. J. Hydrogen Energy 41 (2016) 19637–19644, http://dx.doi.org/10.1016/J.IJHYDENE.2016.04.154.
[20] B. Mecheri, A. Iannaci, A. D'Epifanio, M.J. Nieto-Monge, M.J. Lazaro, S. Licoccia, Iron-based electrocatalysts supported on nanostructured carbon to enhance oxygen reduction in microbial fuel cells, ECS Trans. 72 (2016) 9–15, http://dx.doi.org/10.1149/07230.0009ecst.
[21] C. Santoro, R. Gokhale, B. Mecheri, A. D'Epifanio, S. Licoccia, A. Serov, K. Artyushkova, P. Atanassov, Design of iron(II) phthalocyanine-derived oxygen reduction electrocatalysts for High-power-density microbial fuel cells, ChemSusChem 10 (2017) 3243–3251, http://dx.doi.org/10.1002/cssc.201700851.
[22] M.A. Costa de Oliveira, B. Mecheri, A. D'Epifanio, E. Placidi, F. Arciprete, F. Valentini, A. Perandini, V. Valentini, S. Licoccia, Graphene oxide nanoplatforms to enhance catalytic performance of iron phthalocyanine for oxygen reduction reaction in bioelectrochemical systems, J. Power Sources 356 (2017) 381–388, http://dx.doi.org/10.1016/J.JPOWSOUR.2017.02.009.
[23] M.-T. Nguyen, B. Mecheri, A. Iannaci, A. D'Epifanio, S. Licoccia, Iron/polyindole-based electrocatalysts to enhance oxygen reduction in microbial fuel cells, Electrochim. Acta 190 (2016) 388–395, http://dx.doi.org/10.1016/J.ELECTACTA.2015.12.105.
[24] J. Hu, Y. Dong, X. Chen, H. Zhang, J. Zheng, Q. Wang, X. Chen, A highly efficient catalyst: in situ growth of Au nanoparticles on graphene oxide–Fe3O4 nanocomposite support, Chem. Eng. J. 236 (2014) 1–8, http://dx.doi.org/10.1016/J.CEJ.2013.09.080.
[25] M. Lei, Z.B. Wang, J.S. Li, H.L. Tang, W.J. Liu, Y.G. Wang, CeO2 nanocubes-graphene oxide as durable and highly active catalyst support for proton exchange membrane fuel cell, Sci. Rep. 4 (2015) 7415, http://dx.doi.org/10.1038/srep07415.
[26] K.S. Novoselov, A.K. Geim, S.V. Morozov, D. Jiang, Y. Zhang, S.V. Dubonos, I.V. Grigorieva, A.A. Firsov, Electric Field effect in atomically thin carbon films, Science (80-.) 306 (2004) 666–669, http://dx.doi.org/10.1126/science.1102896.
[27] S. Bae, H. Kim, Y. Lee, X. Xu, J.-S. Park, Y. Zheng, J. Balakrishnan, T. Lei, H. Ri Kim, Y. Il Song, Y.-J. Kim, K.S. Kim, B. Özyilmaz, J.-H. Ahn, B.H. Hong, S. Iijima, Roll-to-roll production of 30-inch graphene films for transparent electrodes, Nat. Nanotechnol. 5 (2010) 574–578, http://dx.doi.org/10.1038/nnano.2010.132.
[28] K.V. Emtsev, A. Bostwick, K. Horn, J. Jobst, G.L. Kellogg, L. Ley, J.L. McChesney, T. Ohta, S.A. Reshanov, J. Röhrl, E. Rotenberg, A.K. Schmid, D. Waldmann, H.B. Weber, T. Seyller, Towards wafer-size graphene layers by atmospheric pressure graphitization of silicon carbide, Nat. Mater. 8 (2009) 203–207, http://dx.doi.org/10.1038/nmat2382.
[29] S. Park, R.S. Ruoff, Chemical methods for the production of graphenes, Nat. Nanotechnol. 4 (2009) 217–224, http://dx.doi.org/10.1038/nnano.2009.58.
[30] K. Parvez, Z.-S. Wu, R. Li, X. Liu, R. Graf, X. Feng, K. Müllen, Exfoliation of graphite into graphene in aqueous solutions of inorganic salts, J. Am. Chem. Soc. 136 (2014) 6083–6091, http://dx.doi.org/10.1021/ja5017156.
[31] K. Parvez, R.A. Rincón, N.-E. Weber, K.C. Cha, S.S. Venkataraman, One-step electrochemical synthesis of nitrogen and sulfur co-doped, high-quality graphene oxide, Chem. Commun. 52 (2016) 5714–5717, http://dx.doi.org/10.1039/C6CC01250G.
[32] F. Lou, M.E.M. Buan, N. Muthuswamy, J.C. Walmsley, M. Rønning, D. Chen, One-step electrochemical synthesis of tunable nitrogen-doped graphene, J. Mater. Chem. A. 4 (2016) 1233–1243, http://dx.doi.org/10.1039/C5TA08038J.
[33] B. Mecheri, A. Iannaci, A. D'Epifanio, A. Mauri, S. Licoccia, Carbon-supported zirconium oxide as a cathode for microbial fuel cell applications, Chempluschem 81 (2016) 80–85, http://dx.doi.org/10.1002/cplu.201500347.
[34] T.P. Sciarria, A. Tenca, A. D'Epifanio, B. Mecheri, G. Merlino, M. Barbato, S. Borin, S. Licoccia, V. Garavaglia, F. Adani, Using olive mill wastewater to improve performance in producing electricity from domestic wastewater by using single-chamber microbial fuel cell, Bioresour. Technol. 147 (2013) 246–253, http://dx.doi.org/10.1016/J.BIORTECH.2013.08.033.
[35] M.-T. Nguyen, B. Mecheri, A. D'Epifanio, T.P. Sciarria, F. Adani, S. Licoccia, Iron chelates as low-cost and effective electrocatalyst for oxygen reduction reaction in microbial fuel cells, Int. J. Hydrogen Energy 39 (2014) 6462–6469, http://dx.doi.org/10.1016/J.IJHYDENE.2014.02.064.
[36] A. Iannaci, T. Pepè Sciarria, B. Mecheri, F. Adani, S. Licoccia, A. D'Epifanio, Power generation using a low-cost sulfated zirconium oxide based cathode in single chamber microbial fuel cells, J. Alloys Compd. 693 (2017) 170–176, http://dx.doi.org/10.1016/J.JALLCOM.2016.09.159.
[37] S. Stankovich, D.A. Dikin, R.D. Piner, K.A. Kohlhaas, A. Kleinhammes, Y. Jia, Y. Wu, S.T. Nguyen, R.S. Ruoff, Synthesis of graphene-based nanosheets via chemical reduction of exfoliated graphite oxide, Carbon N. Y. 45 (2007) 1558–1565, http://dx.doi.org/10.1016/J.CARBON.2007.02.034.
[38] A.C. Ferrari, D.M. Basko, Raman spectroscopy as a versatile tool for studying the properties of graphene, Nat. Nanotechnol. 8 (2013) 235–246, http://dx.doi.org/10.1038/nnano.2013.46.
[39] A.C. Ferrari, Raman spectroscopy of graphene and graphite: disorder, electron–phonon coupling, doping and nonadiabatic effects, Solid State Commun. 143 (2007) 47–57, http://dx.doi.org/10.1016/J.SSC.2007.03.052.
[40] A. Viinikanoja, J. Kauppila, P. Damlin, M. Suominen, C. Kvarnström, In situ FTIR and Raman spectroelectrochemical characterization of graphene oxide upon electrochemical reduction in organic solvents, Phys. Chem. Chem. Phys. 17 (2015) 12115–12123, http://dx.doi.org/10.1039/C5CP00942A.
[41] A.A.K. King, B.R. Davies, N. Noorbehesht, P. Newman, T.L. Church, A.T. Harris, J.M. Razal, A.I. Minett, A New Raman metric for the characterisation of graphene oxide and its derivatives, Sci. Rep. 6 (2016) 19491, http://dx.doi.org/10.1038/srep19491.
[42] S. Claramunt, A. Varea, D. López-Díaz, M.M. Velázquez, A. Cornet, A. Cirera, The importance of interbands on the interpretation of the Raman spectrum of graphene oxide, J. Phys. Chem. C 119 (2015) 10123–10129, http://dx.doi.org/10.1021/acs.jpcc.5b01590.
[43] L.G. Cançado, A. Jorio, E.H.M. Ferreira, F. Stavale, C.A. Achete, R.B. Capaz, M.V.O. Moutinho, A. Lombardo, T.S. Kulmala, A.C. Ferrari, Quantifying defects in graphene via Raman spectroscopy at different excitation energies, Nano Lett. 11 (2011) 3190–3196, http://dx.doi.org/10.1021/nl201432g.
[44] A. Sadezky, H. Muckenhuber, H. Grothe, R. Niessner, U. Pöschl, Raman microspectroscopy of soot and related carbonaceous materials: spectral analysis and structural information, Carbon N. Y. 43 (2005) 1731–1742, http://dx.doi.org/10.1016/J.CARBON.2005.02.018.
[45] S. Vollebregt, R. Ishihara, F.D. Tichelaar, Y. Hou, C.I.M. Beenakker, Influence of the growth temperature on the first and second-order Raman band ratios and widths of carbon nanotubes and fibers, Carbon N. Y. 50 (2012) 3542–3554, http://dx.doi.org/10.1016/J.CARBON.2012.03.026.
[46] G. Shao, Y. Lu, F. Wu, C. Yang, F. Zeng, Q. Wu, Graphene oxide: the mechanisms of oxidation and exfoliation, J. Mater. Sci. 47 (2012) 4400–4409, http://dx.doi.org/10.1007/s10853-012-6294-5.
[47] Y. Chen, R. Ma, Z. Zhou, G. Liu, Y. Zhou, Q. Liu, S. Kaskel, J. Wang, An in situ source-template-interface reaction route to 3D nitrogen-doped hierarchical porous carbon as oxygen reduction electrocatalyst, Adv. Mater. Interfaces. 2 (2015) 1500199, , http://dx.doi.org/10.1002/admi.201500199.
[48] B. Kumar, M. Asadi, D. Pisasale, S. Sinha-Ray, B.A. Rosen, R. Haasch, J. Abiade, A.L. Yarin, A. Salehi-Khojin, Renewable and metal-free carbon nanofibre catalysts for carbon dioxide reduction, Nat. Commun. 4 (2013) 2819, http://dx.doi.org/10.1038/ncomms3819.
[49] L. WANG, M. Toyoda, M. Inagaki, Dependence of electric double layer capacitance of activated carbons on the types of pores and their surface areas, New. Carbon

Mater. 23 (2008) 111–115, http://dx.doi.org/10.1016/S1872-5805(08)60015-3.
[50] Y. Liu, H. Liu, C. Wang, S.-X. Hou, N. Yang, Sustainable energy recovery in wastewater treatment by microbial fuel cells: stable power generation with nitrogen-doped graphene cathode, Environ. Sci. Technol. 47 (2013) 13889–13895, http://dx.doi.org/10.1021/es4032216.
[51] A. Serov, K. Artyushkova, N.I. Andersen, S. Stariha, P. Atanassov, Original mechanochemical synthesis of Non-platinum group metals oxygen reduction reaction catalysts assisted by sacrificial support method, Electrochim. Acta 179 (2015) 154–160, http://dx.doi.org/10.1016/J.ELECTACTA.2015.02.108.
[52] G.V. Zhutaeva, V.A. Bogdanovskaya, E.S. Davydova, L.P. Kazanskii, M.R. Tarasevich, Kinetics and mechanism of oxygen electroreduction on Vulcan XC72R carbon black modified by pyrolysis products of cobalt 5,10,15,20-tetrakis(4-methoxyphenyl)porphyrine in a broad pH interval, J. Solid State Electrochem. 18 (2014) 1319–1334, http://dx.doi.org/10.1007/s10008-013-2233-x.
[53] B.I. Kharisov, O.V. Kharissova, A. Vázquez Dimas, I. Gómez De La Fuente, Y. Peña Méndez, Review: graphene-supported coordination complexes and organometallics: properties and applications, J. Coord. Chem. 69 (2016) 1125–1151, http://dx.doi.org/10.1080/00958972.2016.1170817.
[54] H. Yin, C. Zhang, F. Liu, Y. Hou, Hybrid of iron nitride and nitrogen-doped graphene aerogel as synergistic catalyst for oxygen reduction reaction, Adv. Funct. Mater. 24 (2014) 2930–2937, http://dx.doi.org/10.1002/adfm.201303902.
[55] J.-H. Yang, Y. Gao, W. Zhang, P. Tang, J. Tan, A.-H. Lu, D. Ma, Cobalt Phthalocyanine–graphene oxide nanocomposite: complicated mutual electronic interaction, J. Phys. Chem. C 117 (2013) 3785–3788, http://dx.doi.org/10.1021/jp311051g.
[56] D. Li, Z. Peng, L. Deng, Y. Shen, Y. Zhou, Theoretical studies on molecular structure and vibrational spectra of copper phthalocyanine, Vib. Spectrosc. 39 (2005) 191–199, http://dx.doi.org/10.1016/J.VIBSPEC.2005.03.004.
[57] S. Singh, S.K. Tripathi, G.S.S. Saini, Effect of pyridine on infrared absorption spectra of copper phthalocyanine, Spectrochim. Acta Part A Mol. Biomol. Spectrosc. 69 (2008) 619–623, http://dx.doi.org/10.1016/J.SAA.2007.05.012.
[58] S. Singh, S.K. Tripathi, G.S.S. Saini, Optical and infrared spectroscopic studies of chemical sensing by copper phthalocyanine thin films, Mater. Chem. Phys. 112 (2008) 793–797, http://dx.doi.org/10.1016/J.MATCHEMPHYS.2008.06.044.
[59] D. Verma, R. Dash, K.S. Katti, D.L. Schulz, A.N. Caruso, Role of coordinated metal ions on the orientation of phthalocyanine based coatings, Spectrochim. Acta Part A Mol. Biomol. Spectrosc. 70 (2008) 1180–1186, http://dx.doi.org/10.1016/J.SAA.2007.10.050.
[60] C. Zhang, R. Hao, H. Yin, F. Liu, Y. Hou, Iron phthalocyanine and nitrogen-doped graphene composite as a novel non-precious catalyst for the oxygen reduction reaction, Nanoscale 4 (2012) 7326, http://dx.doi.org/10.1039/c2nr32612d.
[61] T. Li, Y. Peng, K. Li, R. Zhang, L. Zheng, D. Xia, X. Zuo, Enhanced activity and stability of binuclear iron (III) phthalocyanine on graphene nanosheets for electrocatalytic oxygen reduction in acid, J. Power Sources 293 (2015) 511–518, http://dx.doi.org/10.1016/J.JPOWSOUR.2015.05.099.
[62] Y. Liu, Y.-Y. Wu, G.-J. Lv, T. Pu, X.-Q. He, L.-L. Cui, Iron(II) phthalocyanine covalently functionalized graphene as a highly efficient non-precious-metal catalyst for the oxygen reduction reaction in alkaline media, Electrochim. Acta 112 (2013) 269–278, http://dx.doi.org/10.1016/J.ELECTACTA.2013.08.174.
[63] B. Li, X. Zhou, X. Wang, B. Liu, B. Li, Hybrid binuclear-cobalt-phthalocyanine as oxygen reduction reaction catalyst in single chamber microbial fuel cells, J. Power Sources 272 (2014) 320–327, http://dx.doi.org/10.1016/J.JPOWSOUR.2014.08.058.
[64] Y. Ren, D. Pan, X. Li, F. Fu, Y. Zhao, X. Wang, Effect of polyaniline-graphene nanosheets modified cathode on the performance of sediment microbial fuel cell, J. Chem. Technol. Biotechnol. 88 (2013) 1946–1950, http://dx.doi.org/10.1002/jctb.4146.